proceedings

MDPI

Proceedings

Dual Mode Radiation Sensor for UAS Platforms †

Alexander Barzilov * and Monia Kazemeini

Department of Mechanical Engineering, University of Nevada Las Vegas, Las Vegas, NV 89154, USA;
* Correspondence: alexander.barzilov@unlv.edu

† Presented at the 6th International Electronic Conference on Sensors and Applications, 15–30 November 2019; Available online: https://ecsa-6.sciforum.net/

Published: 14 November 2019

Abstract: Remote sensing technologies are important for radiation safety and environmental security applications. A dual mode Cs2LiYCl$_6$:Ce^{3+} (CLYC) sensor was developed for simultaneous neutron measurements and gamma-ray spectroscopy. To keep users away from hazardous areas, an unmanned aerial system was used as a mobile sensor platform. The sensor was integrated into a multicopter platform as a 'plug and fly' component allowing deployment in the field conditions. The photon energy resolution of the CLYC sensor was measured as less than 5% at 662 keV. The detection of neutrons was achieved via ^{6}Li(n,α)t reaction. The sensor's signal communication and data fusion was programmed using Robot Operating System framework, as well as on-board signal analysis functions including the neutron-photon pulse shape discrimination and the identification of photo peaks in the gamma spectrum. These data with added real time kinematic GPS and time stamps were reported to the user enabling real time awareness of the monitored area, further analysis in temporal and spatial domains, and also radiation mapping and source search tasks.

Keywords: radiation sensor; dual mode; neutrons; gamma rays; unmanned aerial system

1. Introduction

Evaluation of radiological contamination in hazardous zones that may be hard to reach is important for environmental security and radiation safety missions. Sources of ionizing radiation can be displaced or lost [1,2] causing the dose delivered to public and workers. Radioactive isotopes can be released into the environment as a result of accidents at nuclear facilities or natural disasters that affect the critical infrastructure such as spent fuel and reactor installations. The accident at Fukushima Daiichi nuclear power plant that followed the earthquakes and tsunami caused radiological contamination of this facility and neighboring zones, including the ocean water [3]. The use of monitoring robots equipped with the radiation sensing and navigation means allows inspecting these zones remotely, including wide areas, hence decreasing the operator's radiation exposure risks.

Unmanned aerial systems (UAS) can be utilized as mobile robotic platforms to carry photon and neutron sensors for measurements in the field [4,5]. The UAS enables dynamic tracking of the measured radiation flux. This data can be used for radiation contamination analysis in space and time, e.g. for mapping of unsafe zones [6]. Cooperative sensing can be achieved using several UAS: such as mapping of the borders of a contaminated zone or localization of lost sources. In order to make these applications possible, radiation sensors and supporting components should be integrated into the robotic system taking into account the available power. For the use of sensor-equipped UAS in the field, it is desirable to design the 'plug and fly' option of hot plugging and unplugging of the sensors into a platform [7]. Moreover, limited data transmission capabilities of the UAS should be addressed in the sensor design – the analysis of measured signals should be automatically completed onboard extracting the important information only to decrease the size of data packages that are transmitted from the aerial system to a ground station or to other drones.

In remote sensing, gamma and neutron radiation is of interest. Typically, separate sensors were employed for detection and quantification of these two radiation types. Simultaneous detection of photons and neutrons by a single sensor is required in order to decrease the size, weight, and power of the UAS based sensor's package. Such dual mode detectors were studied for neutron-photon imaging systems, for example [8]. To address this need, a $Cs_2LiYCl_6:Ce^{3+}$ (CLYC) sensor was designed for neutron detection and photon spectroscopy. The CLYC scintillator can function in ambient temperature settings without cryogenic cooling which is important for deployment in the field. The sensor was integrated into an UAS platform.

2. Materials and Methods

2.1. UAS Platform

The octocopter kit DJI-S1000 [9] was used as the UAS platform frame for this project (see Figure 1). The octocopter has a diagonal wheelbase of 104.5 cm, 38.6 cm long frame arms, and 38 cm diameter propellers. Eight 4114 400 KV electric motors were mounted on each arm of the octocopter's frame. The UAS weight is 4.4 kg. The platform allows to attach a 6.8 kg payload. With the 8000 mAh 6S lithium battery, the fully loaded UAS can fly 15 minutes. Its landing gear can be raised in flight. It contains several onboard sensors and devices.

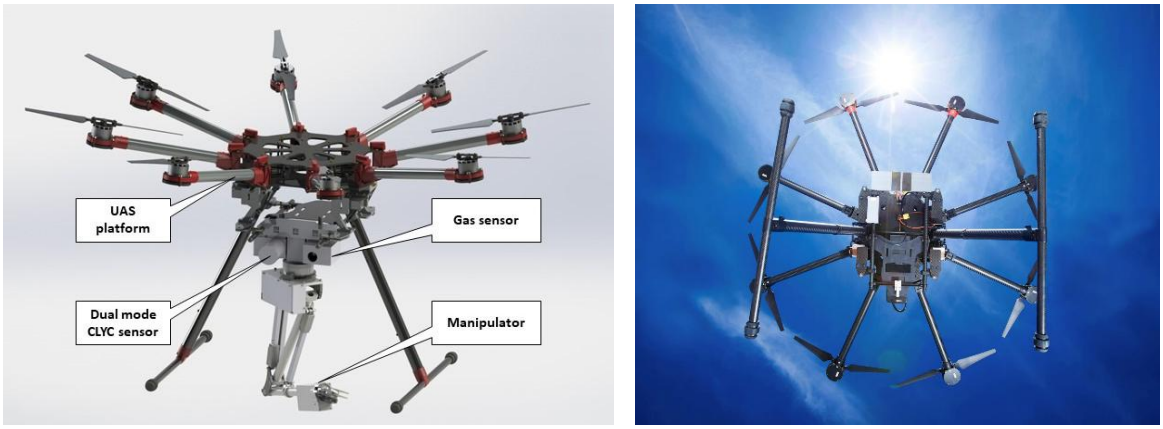

(**a**) (**b**)

Figure 1. DJI-S1000 octocopter: (**a**) 3D rendering of UAS frame with the attached payload; (**b**) a view of the aerial robotic platform.

The octocopter can be controlled by an operator by means of an RC control or a ground station computer with a graphical user interface (GUI) that enables executing the UAS applications. Commands generated by the ground station computer's GUI are enacted on the platform's onboard Linux minicomputer (the Odroid model) that runs Robot Operating System (ROS) [10]. ROS is a framework for robotic applications. It includes libraries and tools consisting of a number of nodes communicating with each other using a publishing or subscribing messaging model. The Odroid serves as the UAS's central data hub and controls the dual mode radiation sensor, a gas sensor, a Hokuyo Lidar, and a 3DR radio transceiver. It is also connected to the Pixhawk 2.1 flight controller that incorporates the isolated and dampened components - a flight management unit and an inertial measurement unit with a built-in heating system and robust connectors that help to resist shocks and diminish the noise. Low-level flight control is executed by the Pixhawk.

Reference velocities data can be sent through the Odroid; the position feedback data can be supplied by a GPS or the PX4 Flow (a combined optic flow and sonar sensor) and may be used where GPS data is unavailable, i.e. in indoor missions. The Lidar sensor enables obstacle avoidance methods during the autonomous operation. The radiation data streamed by the CLYC sensor was time stamped and fused with the UAS's position data based on the real time kinematic (RTK) GPS positioning technology. The RTK GPS is a navigation technique that enhances the precision of

position data derived from satellite-based positioning systems. It is based on measurements of the phase of the signal's carrier wave using a single reference station to provide the real time corrections [11]. The base station with known coordinates has a fixed Swift Duro GPS Receiver. The aerial platform carries a Piksi Multi GPS receiver and L1L2 antenna. Correction data for ionosphere error calculations was transmitted to the GPS Receiver of the UAS platform from the base station.

2.2. CLYC Radiation Sensor

A dual mode CLYC sensor is based on a bright elpasolite scintillator (3.31 g/cm^3 density) that allows for simultaneous neutron and photon sensing by a single detector cell. Depending on the lithium isotopic composition of CLYC, it can be used as a thermal neutron sensor via ^{6}Li(n,α)t reaction (thermal-neutron's signature at the 3-MeV gamma equivalent energy region) or as a fast neutron sensor via ^{35}Cl(n,p)^{35}S reaction with Q value of 615 keV, or both. In the (n,p) reaction case, the emitted proton's energy equals to 615 keV plus the incident neutron's energy: hence, the neutron energy can be gathered from the measured full energy proton peak value.

As other elpasolite scintillators, CLYC is capable of a gamma-ray spectroscopy [12]. The CLYC gamma-ray energy resolution is less than 5% at 662 keV. The CLYC's scintillation yield is 2×10^4 photons per 1-MeV gamma ray absorbed, and 7×10^4 photons per the absorbed neutron. The wavelength of scintillation light produced by the CLYC spreads from 275 nm to 450 nm with the peak that is centered at 370 nm. Its refractive index is 1.8 at 405 nm. The process of scintillation in the CLYC volume has distinct decay components: core-to-valence luminescence (CVL, 250 nm - 350 nm wavelength range, 2-ns decay time constant), Ce^{3+} prompt emission (350 nm - 450 nm range; 50-ns decay constant), and cerium self-trapped excitation (Ce-STE, 1-μs decay constant). The last decay component is due to the neutron induced reaction. The first two components are due to photon induced processes in the CLYC. Decay time differences allow for a neutron-photon pulse shape discrimination (PSD) [13].

The dual mode sensor package was designed using a 2.54 cm diameter, 2.54 cm long cylindrical CLYC cell. It was equipped with a super bialkali photomultiplier tube (rated for CLYC's scintillation wavelengths) and a high voltage generator. A miniature emorpho digitizer connected through the USB cable to the Odroid was utilized for processing of sensor's signals. The sensor's scheme and the assembled sensor are shown in Figure 2(a) and Figure 2(b). The components of the sensor were packaged in a plastic housing designed to be easily attached to the robotic platform. The typical waveforms of digitized neutron and gamma induced signals in the CLYC cell are presented in Figure 3. These waveforms were analyzed providing three values recorded in a list mode: (1) a signal's starting time, (2) an integral calculated under the whole waveform that is proportional to the energy of absorbed radiation, and (3) an integral calculated under the front part of the waveform. These list mode data were used for the PSD analysis. The radiation identification (ID) value was evaluated for each waveform as a ratio of the areas under its tail part and front part; it was used to segregate waveforms into two groups: neutron events and photon events. Neutron waveforms have longer tails that the gamma-ray waveforms, thus producing greater ID values.

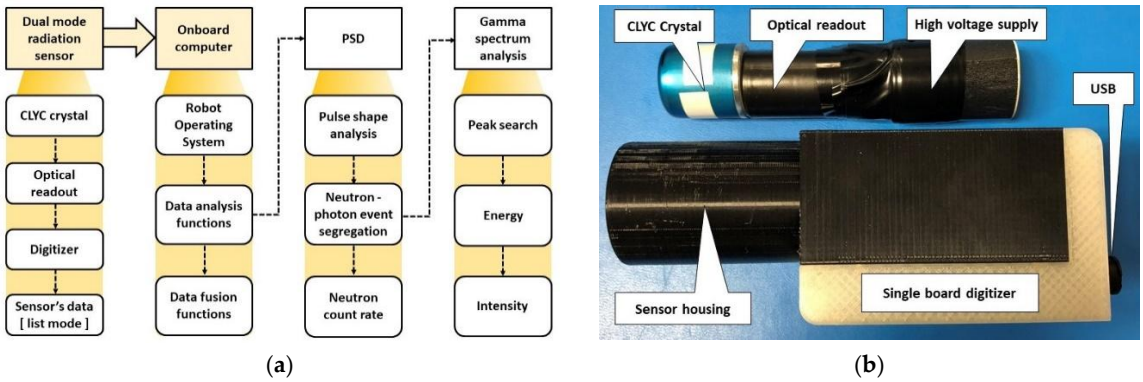

Figure 2. (**a**) Scheme of the dual mode CLYC sensor; (**b**) The assembled sensor's package.

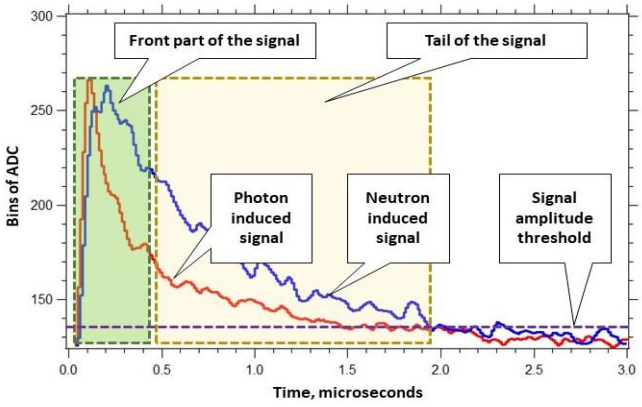

Figure 3. CLYC's neutron and gamma-ray waveforms.

3. Results and Discussion

3.1. Sensor Integration into a Robotic Platform

The 'plug and fly' method was used for the sensor integration into the aerial robotic platform. It enables 'hot plugging' and 'hot unplugging' of the CLYC sensor into the USB interface of UAS. When the CLYC sensor is plugged in and powered on, the operating system (OS) identifies its type. Then OS installs a sensor's driver, starts the measurement, processes and analyzes the measured data, and publishes it. The scheme of plug and fly sensor operation within ROS is shown in Figure 4(a). The CLYC sensor was tested in the plug and fly mode using ROS. Figure 4(b) illustrates the driver processes and sensor's data stream including the time and RTK GPS data fused with the sensor's readings. The RTK GPS system enables raw data measurement rates up to 20 Hz, and RTK position outputs up to 10 Hz. The measured RTK GPS positioning accuracy was within 2 cm.

3.2. Dual Mode Radiation Measurements

The diagram of CLYC's neutron-photon PSD measurements using a PuBe (α,n) source is shown in Figure 5(a). The points representing neutron induced reactions are centered around the 3 MeVee (electron equivalents). This diagram shows excellent segregation of neutron and photon waveforms. A figure of merit (FOM) of PSD [14] for CLYC was measured using a plot of sensor's counts versus radiation ID values: the peak separation was divided by the sum of full widths at a half maximum (FWHM) of neutron and photon peaks resulting in a value of 2.3. This PSD algorithm was programmed as a function within ROS using C language. The photon induced signals were segregated from neutron signals through the PSD analysis and used to plot a gamma-ray energy spectrum.

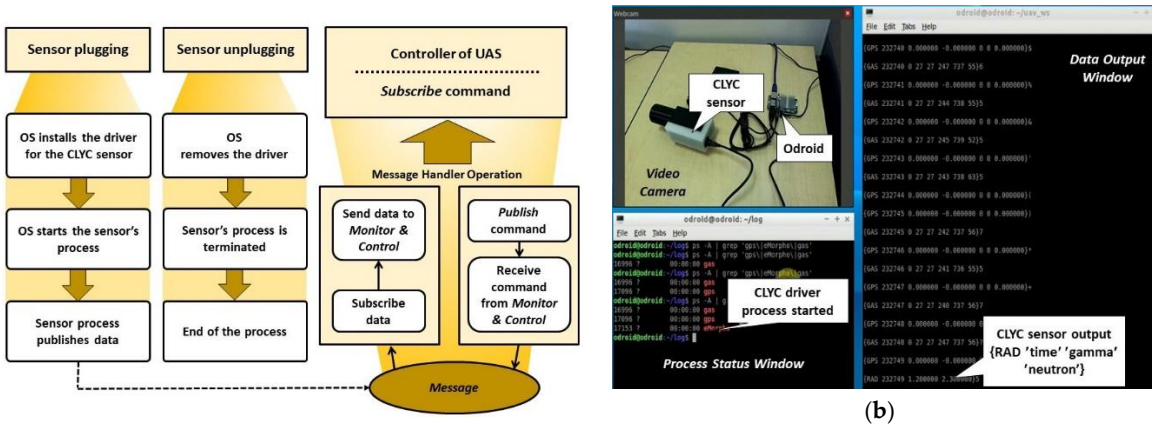

(**a**) (**b**)

Figure 4. (**a**) Scheme of the 'plug and fly' operation of the CLYC sensor; (**b**) Driver processes and sensor's data stream.

The measured FWHM photon energy resolution of the sensor is ~5% at 662 keV, 3.6% at 1173 keV and 3.3% at 1332 keV. of photons emitted by a ^{137}Cs source measured using the CLYC sensor is shown in Figure 5(b). In order to determine the peaks, their centroids and intensities for further identification and quantification of gamma emitters, the spectrum should be automatically processed using spectral analysis algorithms [15,16]. Taking into account the limitations of the onboard Odroid computer, a peak analysis algorithm based on the Mariscotti method [17] was programmed as a function within ROS.

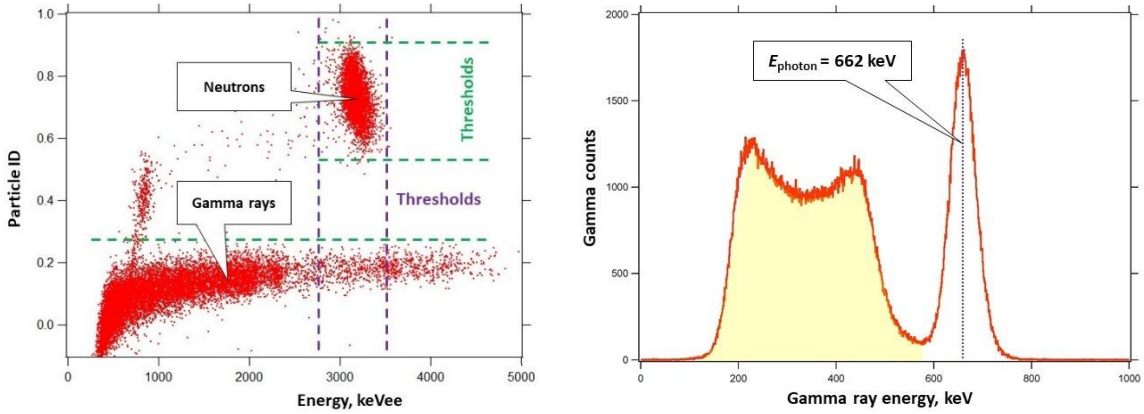

(**a**) (**b**)

Figure 5. (**a**) Neutron-photon PSD diagram of the CLYC sensor measurements in a mixed radiation flux using a PuBe source; (**b**) Photon spectrum recorded by the dual mode sensor using a ^{137}Cs gamma ray source.

4. Conclusion

The $Cs_2LiYCl_6:Ce^{3+}$ dual mode radiation sensor was designed for the use with unmanned aerial systems. This sensor can be utilized for simultaneous measurements of neutrons and gamma rays with an effective pulse shape discrimination of two radiations with the figure of merit of 2.3. The separated photon data enable gamma spectroscopy with energy resolution less than 5% at 662 keV. Sensor was integrated onto the UAS as a 'plug and fly' package using Robot Operating System allowing a user-friendly application in the field settings. Data analysis and fusion functions were programmed within ROS. The time stamped sensor's data were merged with the RTK GPS information.

Author Contributions: Methodology, A.B.; software, M.K.; experiments and analysis, A.B. and M.K.; writing and editing, A.B. and M.K.

Funding: This research was supported by Nuclear Regulatory Commission, the doctoral fellowship grant number NRC-HQ-7P-15-G-0009.

Conflicts of Interest: The authors declare no conflict of interest.

References

1. Till, J.; Grogan, H. *Radiological risk assessment and environmental analysis*; Oxford University Press: New York, 2008. ISBN: 978-0195127270
2. Sen, T.; Moore, L.; Hess, T. An organizational decision support system for managing the DOE hazardous waste cleanup program. *Decis. Support Syst.* **2000**, 29, 89–109. https://doi.org/10.1016/S0167-9236(00)00066-X
3. Nagatani, K.; et al. Emergency response to the nuclear accident at the Fukushima Daiichi nuclear power plants using mobile rescue robots. *J. Field. Robot.* **2013**, *30*, 44–63. https://doi.org/10.1002/rob.21439
4. Barzilov, A.; Hartman, J.; Novikov, I. Remote sensing of neutron and gamma radiation using unmanned aerial system. Proceedings of IEEE, Nuclear Science Symposium and Medical Imaging Conference, San Diego, USA, October 31–November 7 2015; 1–4. https://doi.org/10.1109/NSSMIC.2015.7581763
5. Han, J.; Chen, Y. Multiple UAV formations for cooperative source seeking and contour mapping of a radiative signal field. *J. Intell. Robot. Syst.* **2014**, *74*, 323–332. https://doi.org/10.1007/s10846-013-9897-4
6. Yim, W.; et al. Low-altitude contour mapping of radiation fields using UAS swarm. *Intel. Serv. Robot.* **2019**, *12*, 219–230. https://doi.org/10.1007/s11370-019-00277-8
7. Kazemeini, M.; et al. Plug-and-play radiation sensor components for unmanned aerial system platform. *J. Radioanal Nucl. Ch.* **2018**, *318*, 1797–1803. https://doi.org/10.1007/s10967-018-6233-2
8. Hartman, J.; et al. 3D imaging using combined neutron-photon fan-beam tomography: A Monte Carlo study. *Appl. Radiat. Isotopes.* **2016**, *111*, 110–116. http://dx.doi.org/10.1016/j.apradiso.2016.02.018
9. S1000. Available online: https://www.dji.com/spreading-wings-s1000 (accessed on 5 October 2019).
10. Robot Operating System. Available online: http://www.ros.org (accessed on 5 October 2019).
11. Grejner-Brzezinska, D.; Wielgosz, P.; Kashani, I. On accuracy and reliability of instantaneous network RTK as a function of network geometry, station separation, and data processing strategy. *GPS Solut.* **2005**, *9*, 212–225. http://dx.doi.org/10.1007/s10291-005-0130-1
12. Guss, P.; et al. Scintillation properties of a $Cs_2LiLa(Br_6)90\%$ $(Cl_6)10\%$: Ce^{3+} (CLLBC) crystal. In Proceedings of the SPIE 9215, 2014; 921505. https://doi.org/10.1117/12.2060204
13. D'Olympia, N; et al. Pulse-shape analysis of CLYC for thermal neutrons, fast neutrons, and gamma-rays. *Nucl. Instrum. Meth. A* **2013**, *714*, 121–127. https://doi.org/10.1016/j.nima.2013.02.043
14. Hartman, J.; et al. Measurements of response functions of EJ-299-33A plastic scintillator for fast neutrons. *Nucl. Instrum. Meth. A* **2015**, *804*, 137–143. http://dx.doi.org/10.1016/j.nima.2015.09.068
15. Medhat, M. Artificial intelligence methods applied for quantitative analysis of natural radioactive sources. *Ann. Nucl. Energy* **2012**, *45*, 73–79. https://doi.org/10.1016/j.anucene.2012.02.013
16. Barzilov, A.; Kessler, B., Womble, P. Analysis of 14-MeV neutron induced gamma-ray spectra using multiwavelets. *Radiat. Meas.* **2015**, *79*, 43–49. http://dx.doi.org/10.1016/j.radmeas.2015.06.007
17. Kazemeini, M.; et al. Integration of CZT and CLYC radiation detectors into robotic platforms using ROS. AIP Conference Proceedings 2160, 2019; 050019-1 - 050019-6. https://doi.org/10.1063/1.5127711

© 2019 by the authors; licensee MDPI, Basel, Switzerland. This article is an open access article distributed under the terms and conditions of the Creative Commons Attribution (CC-BY) license (http://creativecommons.org/licenses/by/4.0/).